



Displacement-Controlled Nonlinear Analysis of Offshore Platform Topside Under Accidental Loads

Srinivasan Chandrasekaran¹ · S. Pachaiappan²

Received: 11 January 2022 / Accepted: 24 November 2022 / Published online: 12 December 2022
© King Fahd University of Petroleum & Minerals 2022

Abstract

The offshore platform's topside is vulnerable to accidental loads, including impact and blast loads that arise from hydrocarbon explosions. In addition, higher stresses are developed on members under the wind and wave loads. Recent studies show the effective use of functionally graded materials (FGM) for marine applications under high pressure and temperature. In the current study, FGM comprising carbon-manganese steel and duplex stainless steel is used in members prone to hydrocarbon explosion. Topside with two combinations, FGM and X52 steel, and X52 steel alone are compared. A displacement-controlled nonlinear pushover analysis carried out on the offshore topside with FGM and X52 steel illustrates the advantage of using FGM in probable regions of hydrocarbon explosion. A significant reduction in plastic hinge formations is a clear manifestation of using FGM as the structural material, as it showed increased load capacity compared to X52 steel under lateral loads.

Keywords Topside · Accidental loads · FGM · Hydrocarbon explosion · Pushover analysis

1 Introduction

Offshore platforms are form-dominant steel structures deployed in the deep sea for exploratory drilling, natural gasses, and oil [1–3]. The topside comprises several facilities to support such operations and is subjected to accidental loads, which include impact and blast loads, developing higher stress concentration on structural elements [4–6]. Functionally graded materials (FGM) are suggested for topside application due to their increased strength and performance criteria [7]. The current study examines the capacity of offshore topside under accidental loads using pushover analysis while comparing the response behaviour using FGM and X52 steel. The topside view and details of several components contributing to the load during operation are shown in Fig. 1. Numerical studies carried out using pushover analysis on buildings showed that the response spectrum

method underestimates the building's response compared to the model-pushover analysis [8, 9]. Steel structures under lateral loads are examined to study the effect of concentric bracings on different seismic zones, base shear, roof displacement, and hinge formations [10]. Steel moment-resisting frames with reduced beam section, reduced web section, and fully fixed moment connection are compared to highlight the superiority of the reduced web section. [11]. Braced steel frames showed higher shear capacity [12], but irregularity in the plan shall result in torsional coupling [13]. Offshore topside, as seen in the figure, exhibits a lot of vertical and horizontal irregularities due to the electro-mechanical layout of equipment and pipelines; detailed investigations under accidental loads make the study more important to arrive at a safe design.

Pushover analysis is discussed as an alternate to inelastic seismic analysis. The effect of higher mode contributions and a continuous change in the structure's resistance distribution are elements of uncertainty in the pushover analysis [14]. Modal pushover showed improvement while retaining simplicity over the response spectrum analysis [15–17]. It also contains material nonlinearity under a combined stress state [18]. Ant colony optimization (ACO) is an alternate to estimate the seismic performance of steel frames, which compares well with the genetic algorithm [19]. It is interesting

✉ Srinivasan Chandrasekaran
drsekaran@iitm.ac.in

S. Pachaiappan
pachaiappaniitm@gmail.com

¹ Department of Ocean Engineering, Indian Institute of Technology Madras, Chennai, India

² Department of Civil Engineering, Aditya Engineering College, Surampalem, Andhra Pradesh, India



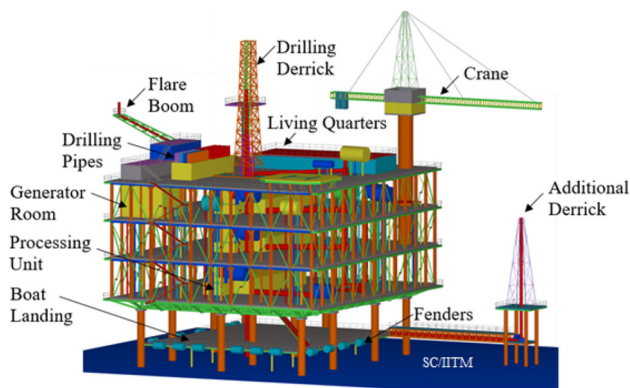


Fig.1 Typical view of offshore platforms topside

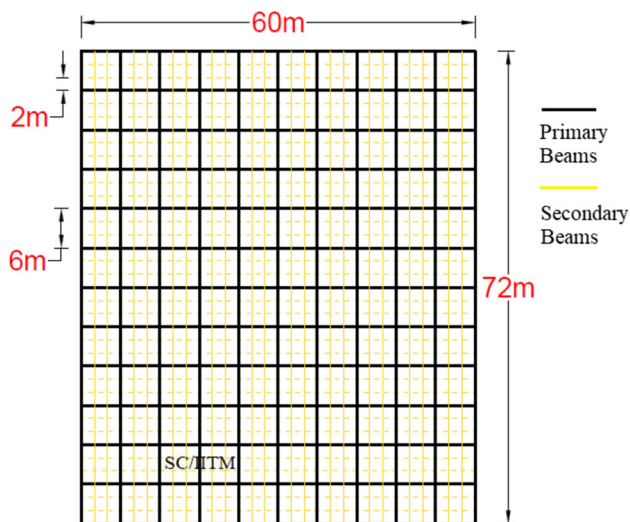


Fig.2 Plan of topside

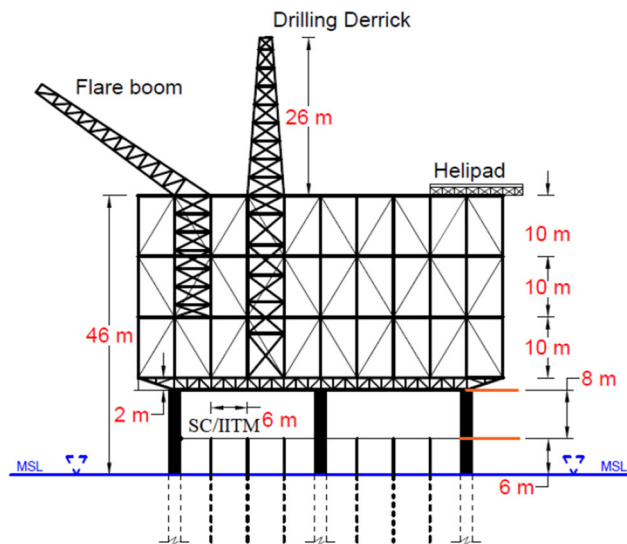


Fig.3 Elevation of topside

Table 1 Topside details [35]

Parameters	Values
Total number of storey	3
Height between floors	10 m
Topside height	46 m
Drilling derrick height	26 m
Storey height (boat landing)	6 m
Materials	X52 steel and FGM
Topside geometry	Symmetrical
Platform dimension	60 m × 72 m
Columns centre to centre distance	6 m
Beams centre to centre distance	2 m
No of bays (X-axis)	10
No of bays (Y-axis)	12
Total dimensions of the deck plate	60 m × 72 m
Deck plate dimension for impact load analysis	6 m × 6 m
Deck plate thickness	17 mm
Stiffeners dimension (T-bar)	100 × 6/36 × 6 mm
Airgap	6 m
Platform Type	Fixed
Geometric reference	Bullwinkle
Significant wave height	4 m

to examine offshore topside under blast loads as the high-temperature effects increase the damage potential, initiating a buckling failure in columns [20–22]. In comparison, the dynamic-based pushover analysis of steel moment-resisting frames shall include higher modes' nonlinear behaviour [23, 24], an improved version of the first mode's participation to yield higher modes, and reported to be more efficient [25–27]. The steel frame's capacity and height affect the behaviour factor (BF) [28, 29], which is also a major concern in offshore topside structures. Further, it is also observed that a lumped plasticity model underestimates the shear demand compared to the shell and frame element model [30–32]. While fire can cause a significant reduction in the mechanical properties of steel at higher temperatures (> 500 °C) [33], a combination of impact and blast loads makes the platform highly vulnerable during installation and operational stages [34]. Blast load raises the temperature in structural members and degrades the beam-column connections. In the presence of accidental loads, waves and wind force combination cause excessive deformation and plastic hinge formations [35]. The present study compares the response behaviour of the topside using pushover analysis under such critical combinations using two different materials, namely X52 steel and FGM. During the blast, the temperature may rise beyond 1000 °C in lesser than

Table 2 Cross-sectional dimensions of structural members [35]

Members	Parameters	Cross-sectional Dimensions (mm)
Columns-(Primary) (Rectangular tubular section)	Depth	820
	Width	460
	Flange thickness	42
	Web thickness	42
Beams-(Primary) (Rectangular tubular section)	Depth	620
	Width	420
	Flange thickness	30
	Web thickness	30
Bracings (Channel section)	Depth	420
	Flange width	160
	Flange thickness	25
	Web thickness	25
Columns supporting boat landing (Tubular section)	Diameter	560
	Wall thickness	45
Deep-beams (Rectangular tubular sections)	Depth	1000
	Width	620
	Flange thickness	50
	Web thickness	50
Columns on buoyant legs (Tubular section)	Diameter	2100
	Wall thickness	180
Topside deck	Thickness	18
Stiffeners (T-section)	Flange	37 × 7
	Web	100 × 6

10 min, causing high thermal stresses [36]. As it is evident that conventional structural steel cannot withstand such high temperatures, the current study examines the use of FGM to model structural members in the region vulnerable to hydrocarbon explosion. FGM constitutes carbon-manganese steel and duplex stainless steel with high resistance to temperature, corrosion, and second-order vibrations, in addition to higher ultimate and yield strength values. A comparative analysis is made between the X52 steel and FGM to show the superiority of FGM under the combination of lateral loads and special loads, which is novel.

2 Geometric Configuration

The topside comprises a multi-tier deck useful for several functional needs. Figures 2 and 3 show the topside plan and elevation; long-span beams and increased storey heights are

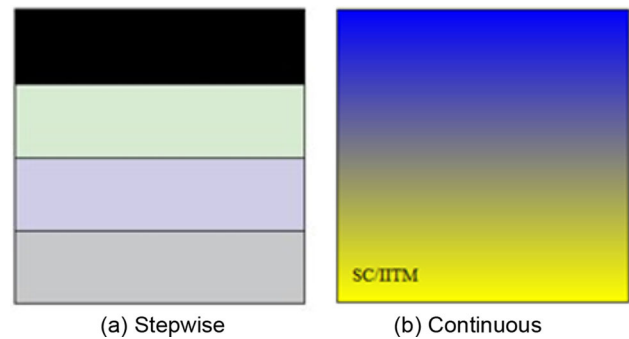


Fig. 4 Functionally graded materials at normal stress conditions [36, 37]

inevitable to facilitate the drilling activities of the topside. The geometry of the Bullwinkle platform deployed in the Gulf of Mexico region at 412 m water depth is taken for reference. A preliminary design is carried out under wave, wind, and mechanical loads; details of the members are summarised in Tables 1 and 2 [35] (Figs. 4 and 5).

3 Materials

Accidental loads occur from a hydrocarbon explosion or high-velocity impact; the strain rate increases rapidly over a finite time, causing a permanent deformation or distortion of the material. Hence, topside material should possess adequate strength, higher resistance to impact loads, good weldability, durability, and toughness. While X52 is the conventional material preferred for topside, the present study explores an alternate material, FGM. Functionally graded materials (FGM) have limited application in offshore platforms but are successful in biomaterials, optics, and energy conversion. FGM possesses improved resistance to second-order vibrations, buckling, and bending, which are demonstrated through three samples; namely, (i) carbon-manganese steel and duplex stainless steel, (ii) Nickel, carbon-manganese steel, and duplex stainless steel, and (iii) titanium, carbon-manganese steel, Nickel, and duplex stainless steel [36, 37]. The material constituents used for fabricating FGM samples in the current study are given in Table 3, while the individual properties of FGM and X52 steel are given in Table 4. The structural members prone to fire accidents are proposed to use FGM, whose section properties are shown in Fig. 6.

4 Wind, Blast, and Impact Load

Wind loads are computed on the topside at every storey level using the gust factor method (GFM). For the mean wind speed

Fig. 5 Stress–strain plot of X52 steel and FGM samples [36, 37]

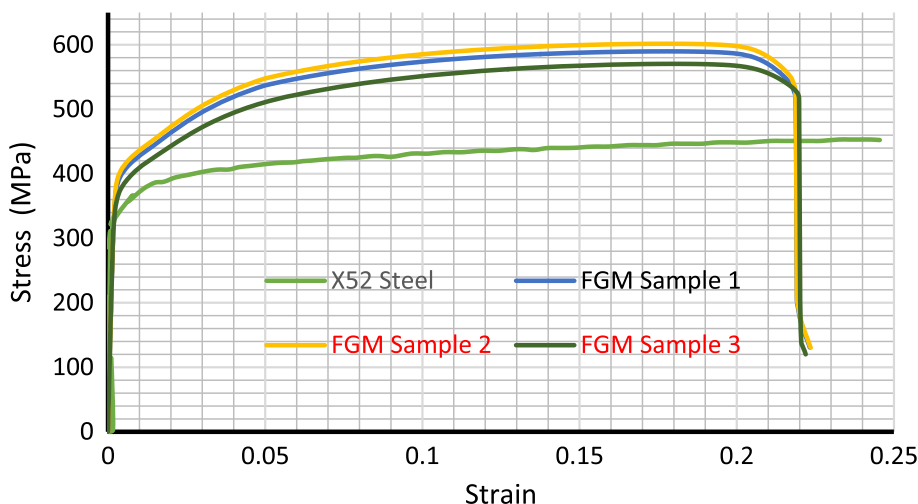


Table 3 Materials properties used for FGM [36, 37]

Properties	Duplex stainless steel	Carbon-manganese steel
Young’s modulus	200 GPa	210 GPa
Poisson ratio	0.30	0.30
Strength ratio	1.55	1.22
Ductility ratio	152	99.14
Unit weight	7800 kg/m ³	7850 kg/m ³

Table 4 Mechanical properties of X52 steel and FGM [36, 37]

Material/Parameter	X52 steel	FGM
Elastic modulus (GPa)	210	209
Yield strength (MPa)	358	390
Ultimate strength (MPa)	453	587
Strength ratio	1.27	1.50
Ductility ratio	32.21	45.46
Tensile toughness (J/m ³)	104	120
Poisson’s ratio	0.30	0.30
Unit weight	7850 kg/m ³	7830 kg/m ³

of 55 m/s (Gulf of Mexico), wind force variation on the top-side is shown in Fig. 7. Wind force on the XZ plane is lesser due to the reduced exposure area, as shown in Fig. 8. Under the payloads recommended by the code [38], the deformation of beams and columns due to the hydrocarbon explosion is computed using ABAQUS explicit. The explosion caused by a blast load is idealized as a linearised triangular impulse, as shown in Fig. 9. The blast pressure is applied on the beams and column surfaces, as shown in Fig. 10. The displacement contour of the beams and columns using X52 steel and FGM are illustrated in Fig. 11, while Figs. 12 and 13 show the beam and column tip displacements. It can be seen from the plots that structural members made of FGM showed reduced displacement in comparison to that of X52 steel due to the improved mechanical properties of FGM.

Impact loads on the topside arise from the fall of machinery, crane hook, equipment, drill pipes, and tools. The fall of objects from a considerable height shall lead to permanent deformation or distortion of the topside deck [39–42]. Figures 14 and 15 show the details of stiffeners used on the topside. In the current study, impact load is generated using the free fall of a square block from a height of about 20 m. The deck plate and stiffeners are shown in Figs. 16 and 17,

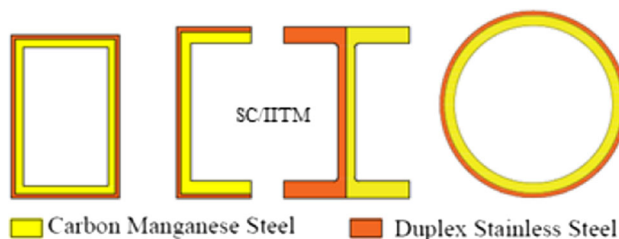


Fig. 6 Structural components proposed for topside using FGM

while Figs. 18 and 19 show a typical offshore crane and the impactor model.

Four-node shell elements are used to model the deck as a 3-D deformable member, while eight are used for the stiffeners. Figure 20 shows the boundary conditions of the topside plate and impactor. Mesh size is optimized for the stiffeners and the deck by following the re-meshing rule. The impactor is modelled as a discrete rigid body, dropped from 20 m height. Numerical analysis is performed by ABAQUS explicit for the time duration of 1000 ms. Figures 21 and 22 show the

Fig. 7 Variation of wind force on the topside [35]

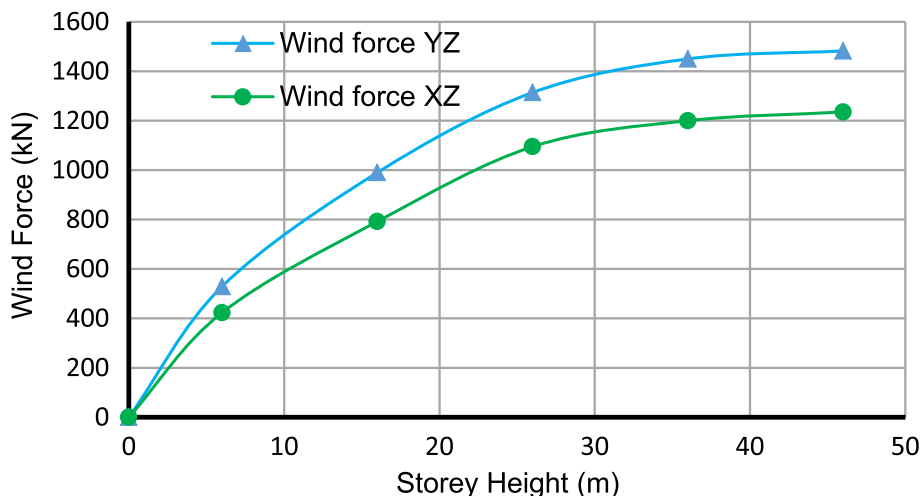


Fig. 8 View of Topside

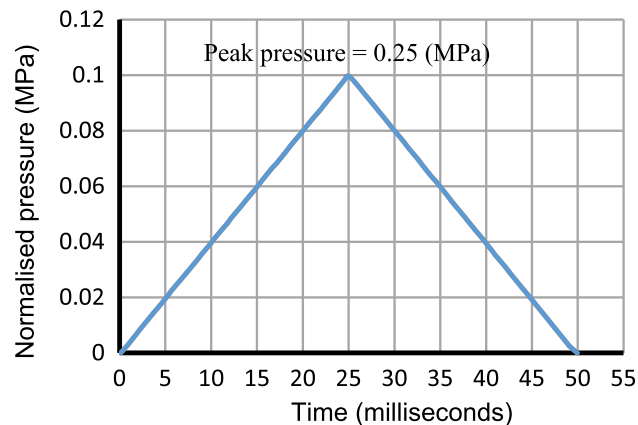
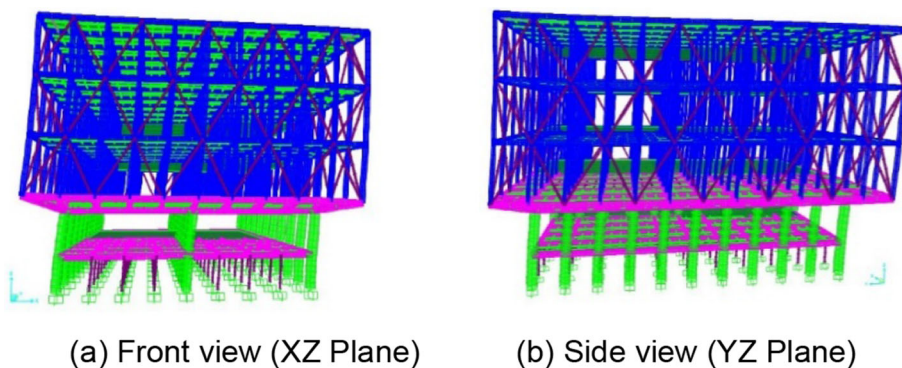


Fig. 9 Triangular blast pressure impulse

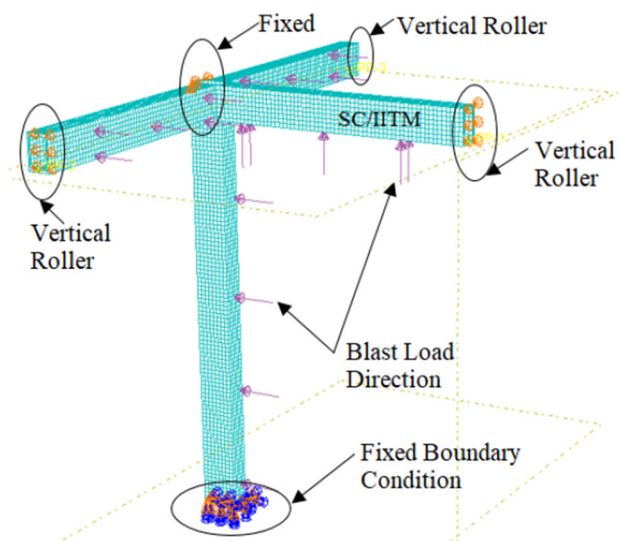


Fig. 10 Direction of blast load and boundary conditions

5 Design of Topside Under Conventional and Accidental Loads

deck’s maximum central deflection for various time steps using FGM and X52 steel under impact load, while Fig. 23 compares their central deflection.

The structural members are chosen based on the topside ultimate load-carrying capacity by considering all the modules

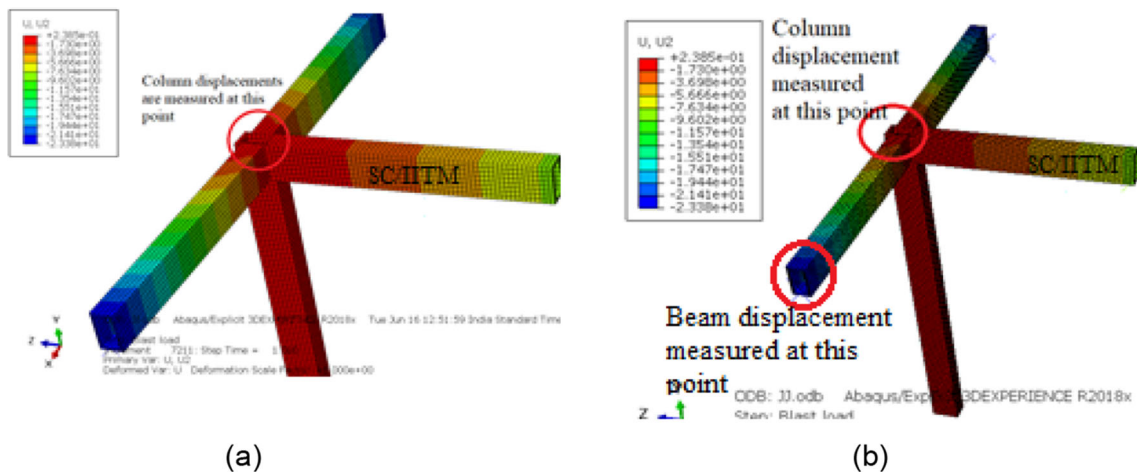


Fig. 11 Displacement contour of beams and columns: **a** X52 steel **b** FGM [35]

Fig. 12 Beam tip displacement comparison at 0.25 MPa [35]

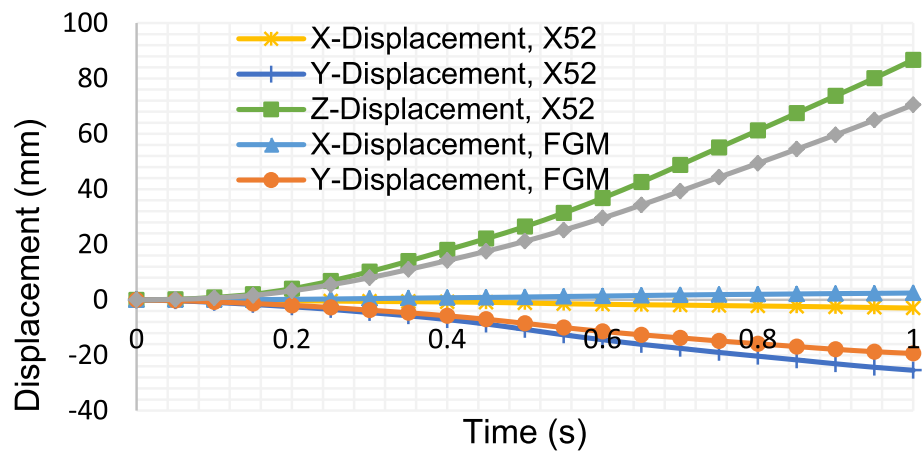
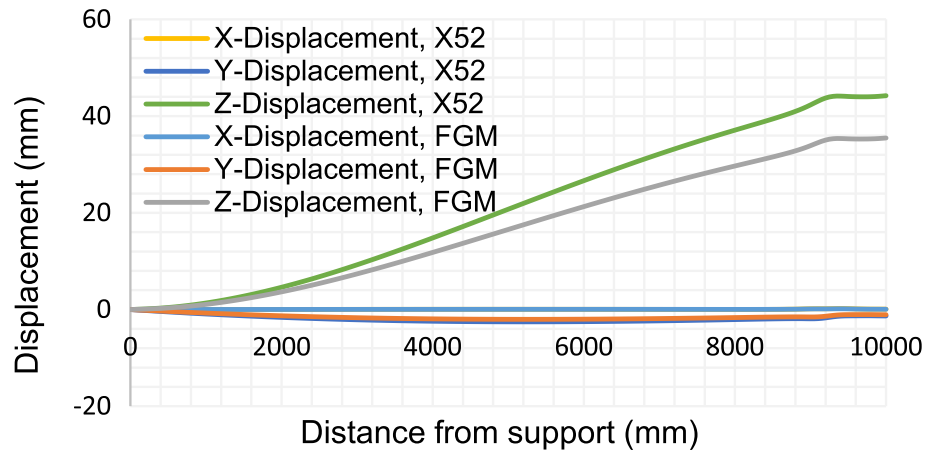


Fig. 13 Column tip displacement comparison at 0.25 MPa [35]



and facilities. Loads on the topside are increased by load factors, complying with the appropriate design codes. IS-800 (2007) and Eurocode 3 (1993) are used for structural member design, and IS-875 (Part 3) is used for wind load calculations. The topside is modelled using SAP 2000 non-linear. Shell elements are used for modelling the deck plate,

while link elements are used for modelling beam-column connections. All support connections are considered rigid connections, while von-mises stress failure criteria are used for the model [35]. The offshore platform’s topside is prone to wind and accidental loads. The accidental load includes the impact and blast from the hydrocarbon explosion. Figure 24

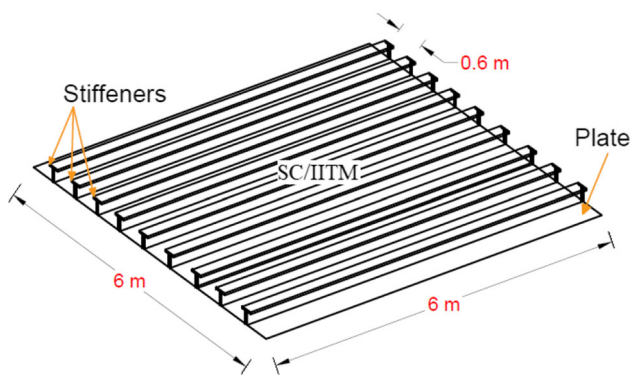


Fig. 14 Typical view of deck plate

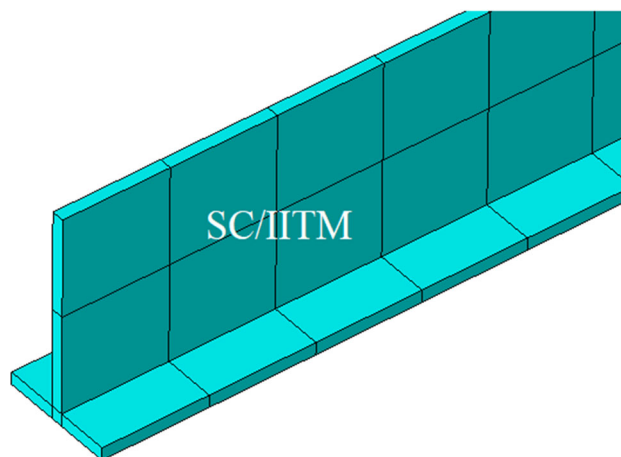


Fig. 17 Model of stiffener

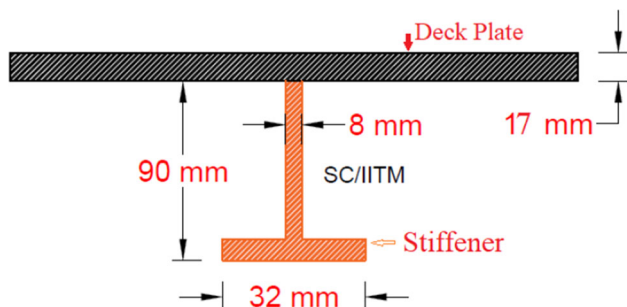


Fig. 15 Stiffeners details

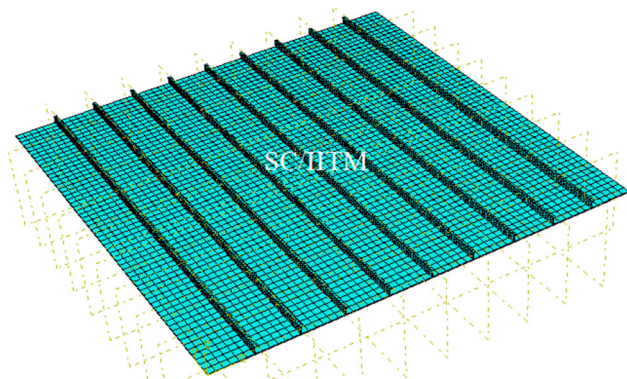


Fig. 16 Model of topside deck plate

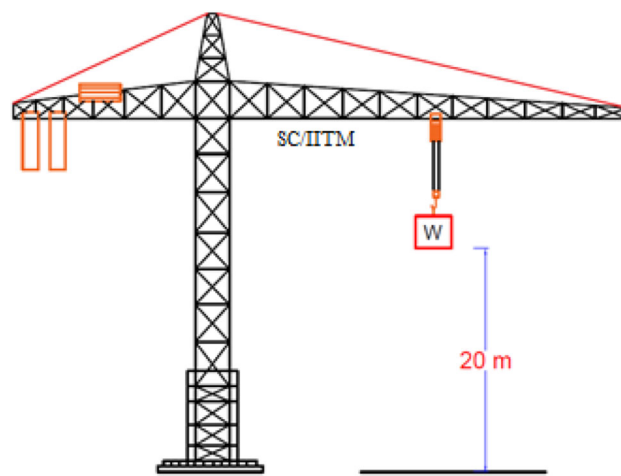


Fig. 18 Typical offshore topside crane

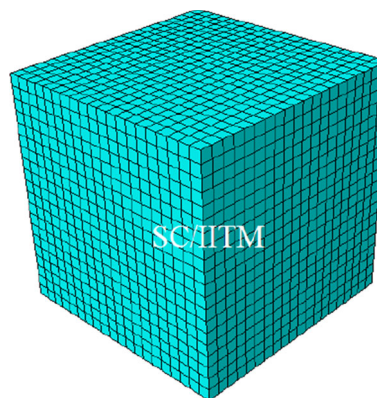


Fig. 19 Model of an impactor

shows the topside’s deformed shape using X52 steel and FGM on selected members in the prone region. Figure 25 shows the deformed shape of the topside using X52 steel. The topside is designed to withstand accidental load and wind combined, while the connections are analysed using ABAQUS. Figure 26 shows the design check carried out on the topside. The revised cross-sectional dimensions of the members based on the design check are shown in Table 5. The topside design satisfies gravity, wind, blast, and impact loads requirements. Further, the topside is investigated by pushover analysis using SAP 2000 nonlinear.

Table 6 shows the dynamic characteristics of the topside for cases 1 and 2. It is seen from the table that natural frequencies for case-1 are marginally higher, indicating higher stiffness of the topside; a higher contribution (about 90%)

Fig. 20 Boundary conditions of the deck plate and Impactor model

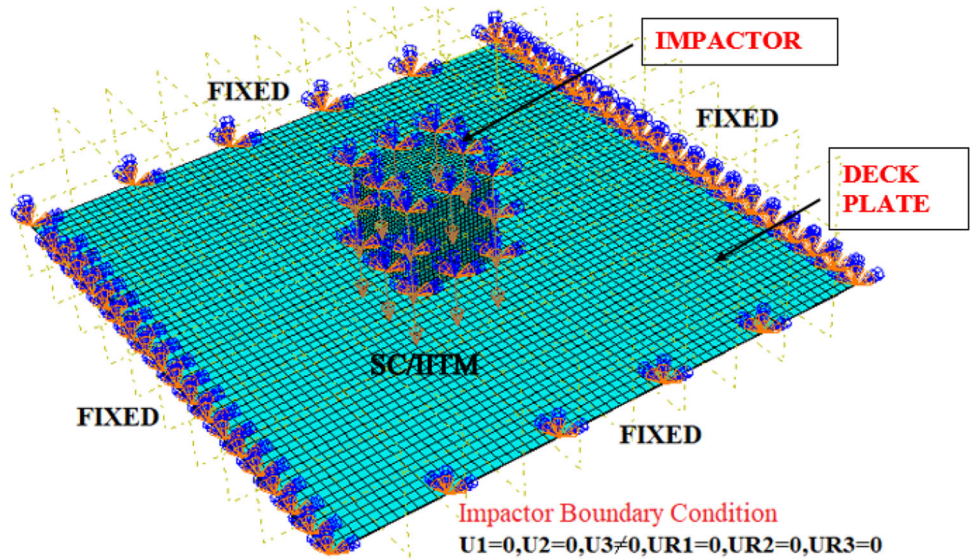
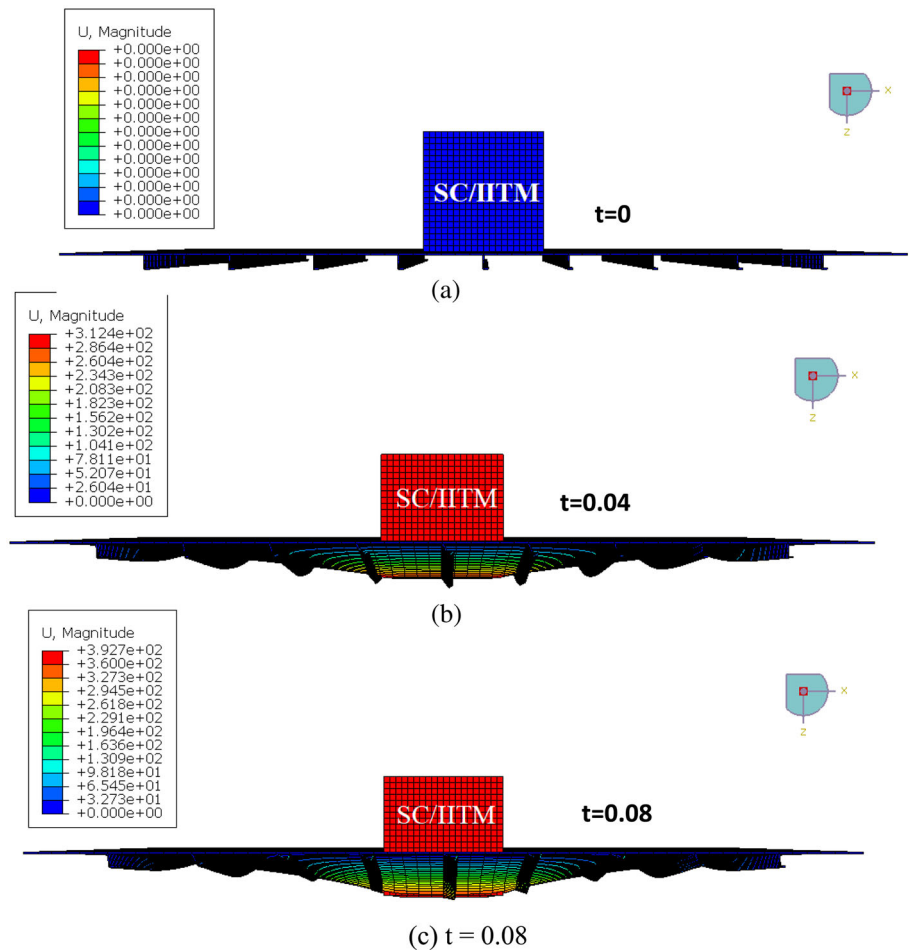


Fig. 21 Deformed shape of the deck with X52 steel



from the first mode indicates an acceptable design. Figures 27 and 28 show the collapse patterns of the topside for case 1 and 2. The first two modes are subjected to lateral vibration, and the third mode shows lateral and torsional vibrations.

Pushover analysis is capable of analysing the topside under lateral forces. A typical topside model is shown in Fig. 29, subjected to gravity loads and predefined lateral load combinations. The lateral forces are distributed along

Fig. 22 Deformed shape of the deck using FGM

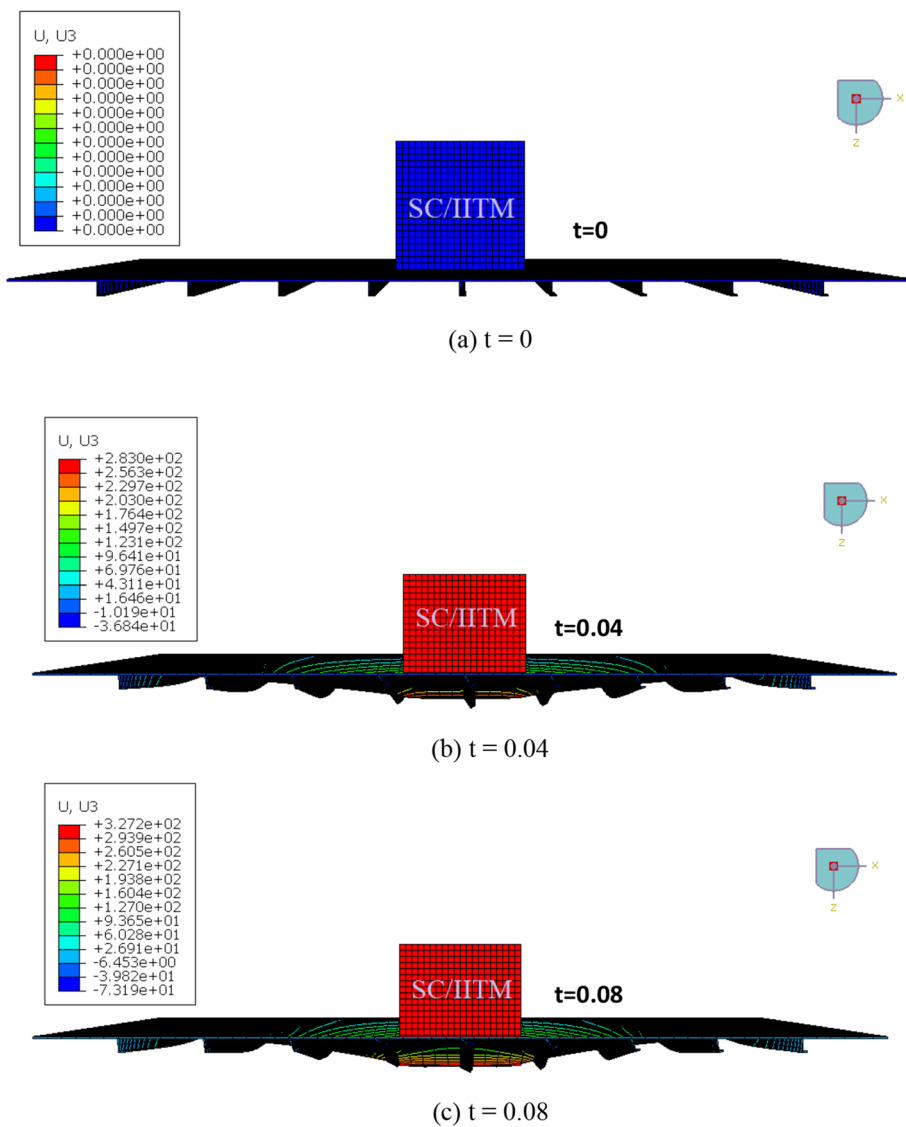


Fig. 23 Comparison of central deflection of the deck

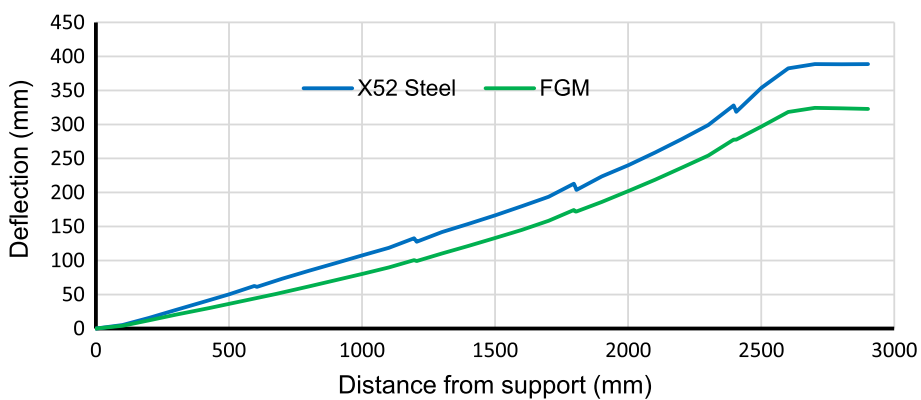


Fig. 24 Topside deformed shape using X52 steel and FGM in a prone region

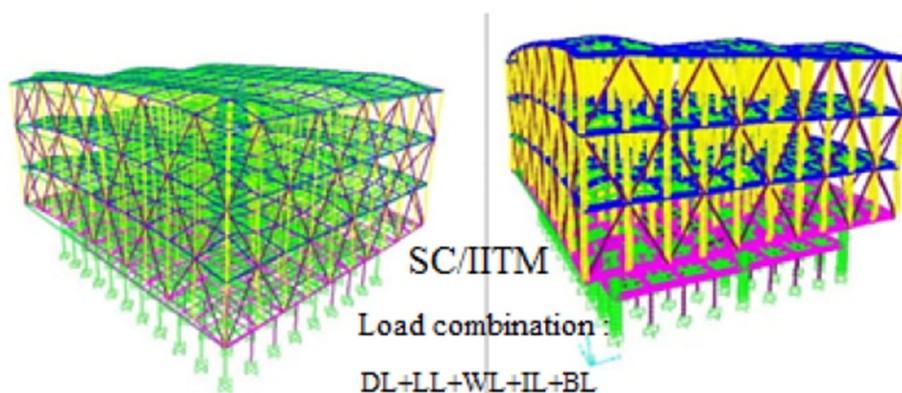


Fig. 25 Topside deformed shape using X52 steel

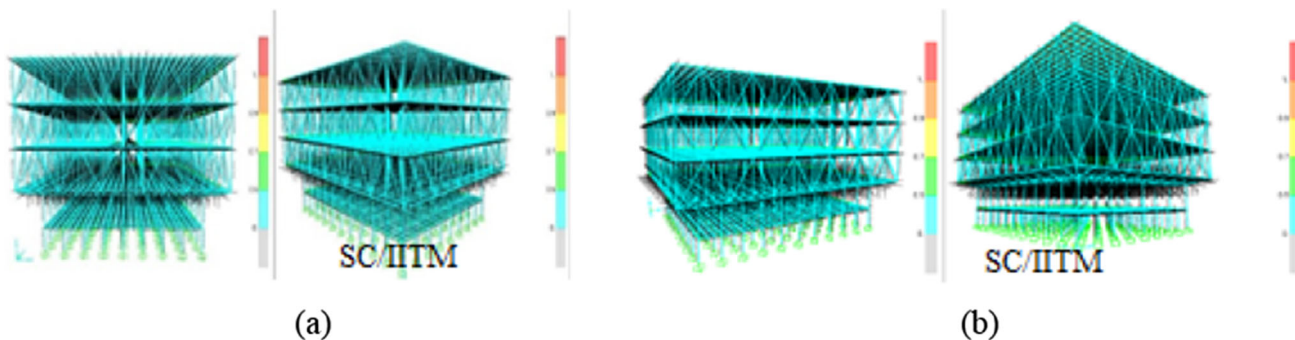
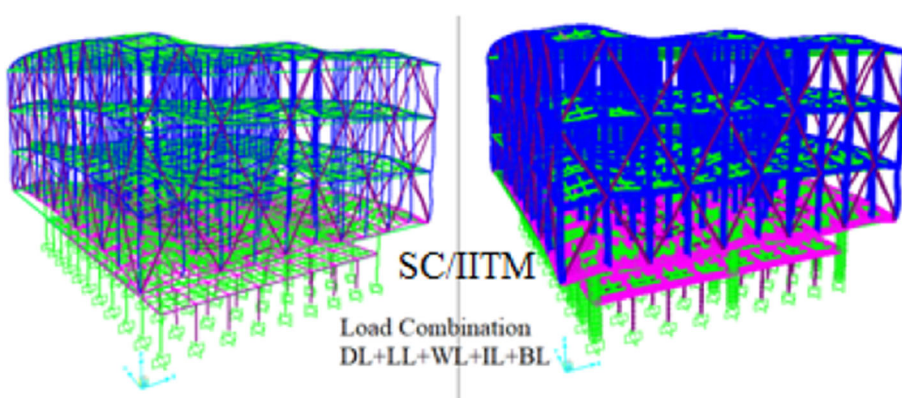


Fig. 26 Design check of the topside: **a** X52 steel and FGM in the prone region; **b** X52 steel

with the height and increased until the yielding of structural members. The structural system is modified to account for a reduced stiffness caused due to the yielding; lateral forces are increased until successive members yield. The process is continued until the structure becomes unstable. The static pushover curve is obtained by plotting the displacement against the base shear. The displacement-controlled pushover analysis (FEMA-356) is used to compute the topside capacity, position of plastic hinge formation, and failure modes. The nonlinear behaviour of the elements is modelled using plastic hinges based on the moment–curvature relationship

as described in FEMA 356 guidelines; P-M2-M3 hinges are used for each structural member. The moment-rotation curve of a P-M2-M3 hinge is a monotonic backbone relationship, which describes the post-yield behaviour of a beam-column element under the combined axial and biaxial-bending conditions. Base shear vs. roof displacement curves are obtained from pushover analysis, as shown in Fig. 31. The intersection of these curves with the seismic demand curve indicates the performance point. It is observed that the lateral displacement under wind and wave is significant in comparison to that of seismic forces. The target displacement was considered

Table 5 Cross-sectional dimensions of members for accidental loads

Members	Parameters	Cross-sectional Dimensions (mm)
Columns-(Primary) (Rectangular tubular section)	Depth	850
	Width	490
	Flange thickness	46
	Web thickness	46
Beams-(Primary) (Rectangular tubular section)	Depth	650
	Width	450
	Flange thickness	35
	Web thickness	35
Bracings (Channel section)	Depth	460
	Flange width	180
	Flange thickness	30
	Web thickness	30
Columns supporting boat landing (Tubular section)	Diameter	800
	Wall thickness	80
Deep-beams (Rectangular tubular sections)	Depth	1200
	Width	800
	Flange thickness	80
	Web thickness	80
Columns on buoyant legs (Tubular section)	Diameter	2100
	Wall thickness	185
Topside deck	Thickness	18.5
Stiffeners (T-section)	Flange	40 × 8
	Web	110 × 8

Table 6 Dynamic characteristics of the topside

Mode	Case-1 (X52 steel + FGM only in prone zones)			Case-2 (X52 for the complete topside)		
	Period (s)	Frequency (rad/s)	Modal participating mass ratio	Period (s)	Frequency (rad/s)	Modal participating mass ratio
1	0.360	17.406	0.810	0.384	16.330	0.81947
2	0.328	19.117	1.95E-06	0.348	18.005	1.48E-06
3	0.311	20.145	1.88E-10	0.328	19.106	1.99E-11
4	0.177	35.480	0.06688	0.188	33.274	0.0572
5	0.167	37.525	2.94E-07	0.182	34.504	1.82E-07
6	0.147	42.595	1.09E-09	0.162	38.551	1.60E-09
7	0.137	45.752	0.01023	0.156	40.253	0.01413
8	0.123	50.851	2.46E-06	0.137	45.708	2.34E-07
9	0.123	50.936	2.09E-07	0.136	45.935	1.74E-07
10	0.113	55.385	1.35E-10	0.123	50.965	2.52E-10
11	0.101	61.696	1.34E-10	0.115	54.382	2.51E-10
12	0.093	67.117	0.00373	0.105	59.348	0.00507

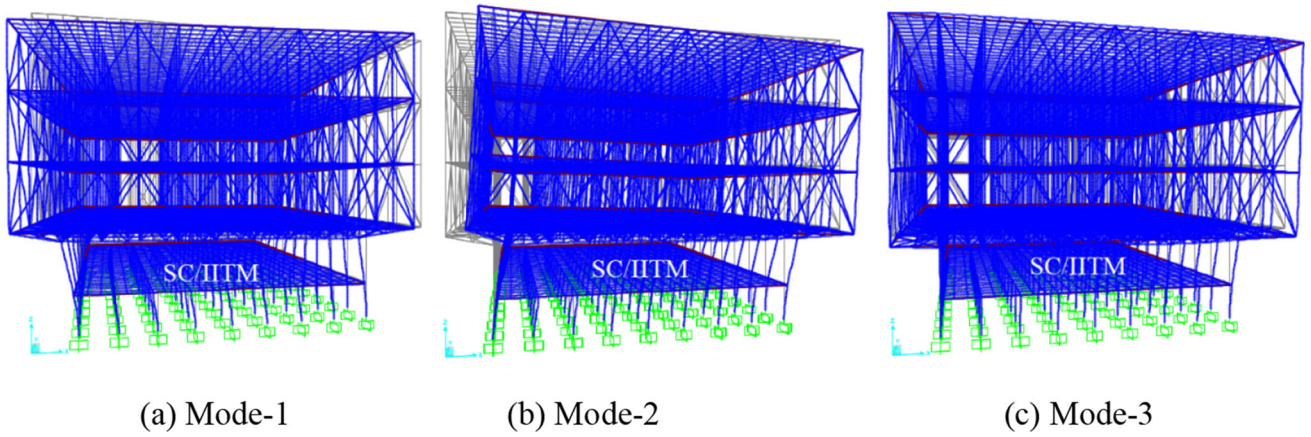


Fig. 27 Collapse pattern of the topside for case-1 (X-52 steel and FGM, used in prone areas)

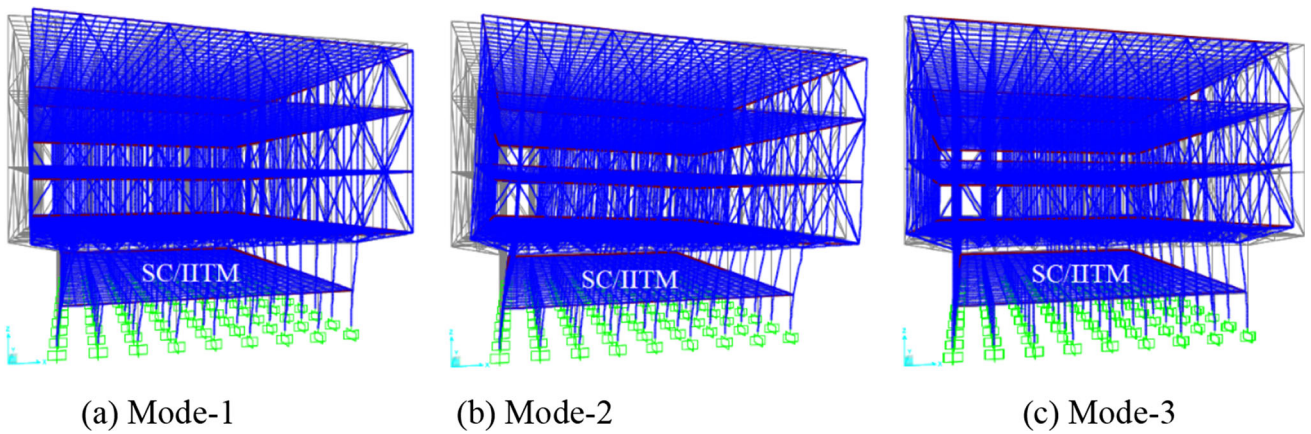


Fig. 28 Collapse pattern of the topside for case-2 (X-52 steel for complete topside)

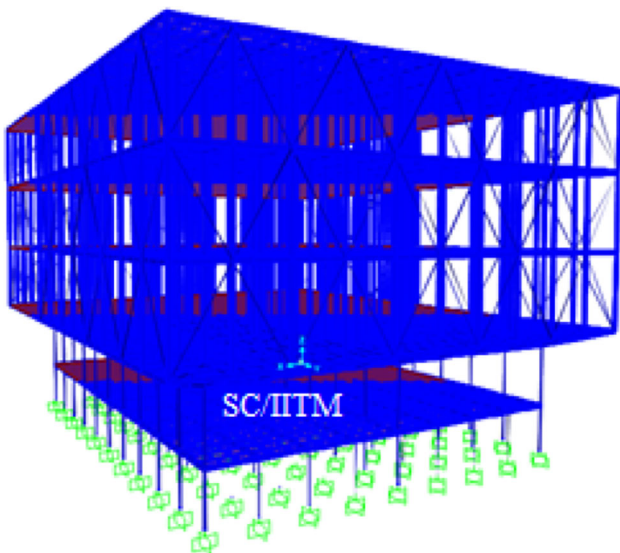


Fig. 29 Typical model of topside

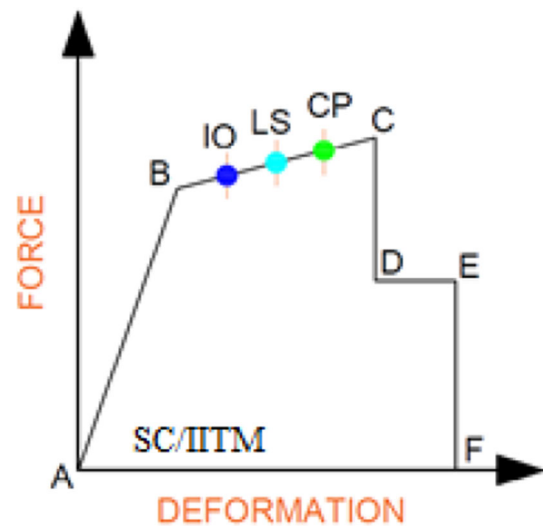


Fig. 30 Idealized pushover curve

Fig. 31 Comparison of pushover curve of Topside for Cases 1 and 2

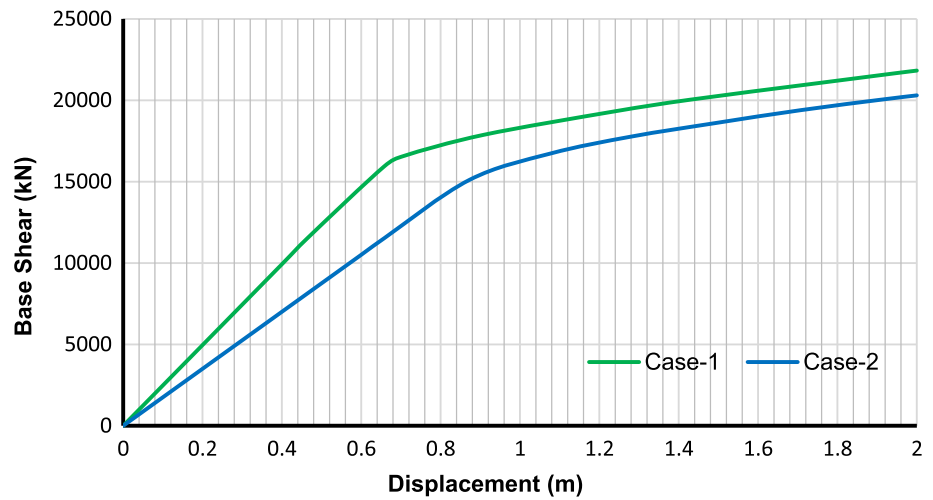


Table 7 Hinge details for case-1

Step	Displacement (m)	Base Shear (kN)	A to B	B to IO	IO to LS	LS to CP	CP to C	C to D	Beyond E
0	0	0	6812	0	0	0	0	0	0
1	0.200	4962	6812	0	0	0	0	0	0
2	0.400	9925	6812	0	0	0	0	0	0
3	0.465	11,543	6812	0	0	0	0	0	0
4	0.657	15,920	6800	12	0	0	0	0	0
5	0.708	16,584	6683	129	0	0	0	0	0
6	0.909	17,878	6110	634	68	0	0	0	0
7	1.231	19,287	5958	208	646	0	0	0	0
8	1.432	20,045	5748	266	798	0	0	0	0
9	1.735	21,001	5738	106	968	0	0	0	0
10	1.945	21,657	5536	226	1050	0	0	0	0
11	2.000	21,822	5486	264	1062	0	0	0	0

Table 8 Hinge details for case-2

Step	Displacement (m)	Base Shear (kN)	A to B	B to IO	IO to LS	LS to CP	CP to C	C to D	Beyond E
0	0	0	6812	0	0	0	0	0	0
1	0.200	3411	6812	0	0	0	0	0	0
2	0.400	6822	6812	0	0	0	0	0	0
3	0.600	10,233	6800	12	0	0	0	0	0
4	0.677	11,544	6332	452	28	0	0	0	0
5	0.895	15,101	6110	634	68	1	0	0	0
6	1.059	16,584	5862	258	692	1	0	0	0
7	1.259	17,658	5738	106	968	3	0	0	0
8	1.427	18,540	5514	244	1054	7	0	0	0
9	1.674	19,286	5486	102	1224	9	1	0	0
10	1.880	19,975	5414	98	1300	9	1	0	0
11	2.000	20,100	5360	152	1300	11	2	0	0

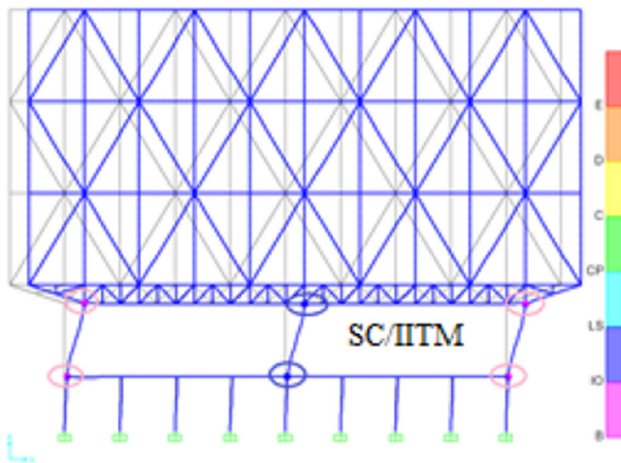


Fig. 32 Location of plastic hinges for case-1

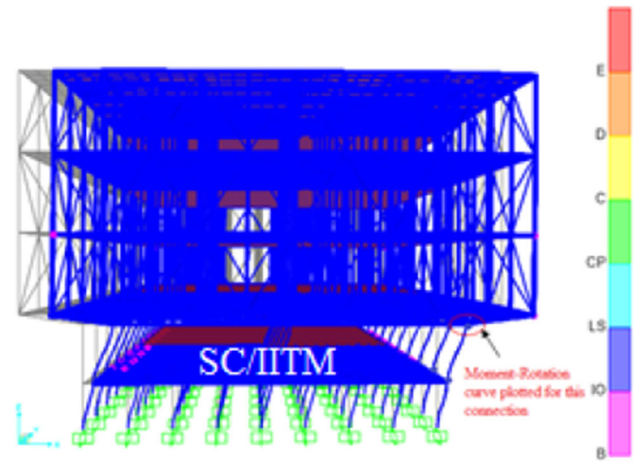


Fig. 34 Collapse pattern of the topside for case-1

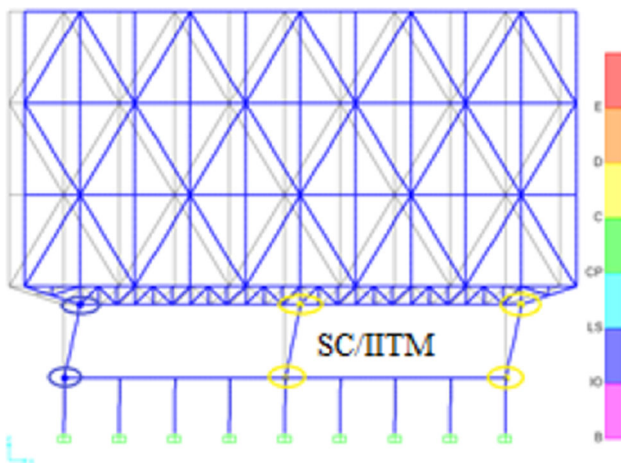


Fig. 33 Location of plastic hinges for case-2

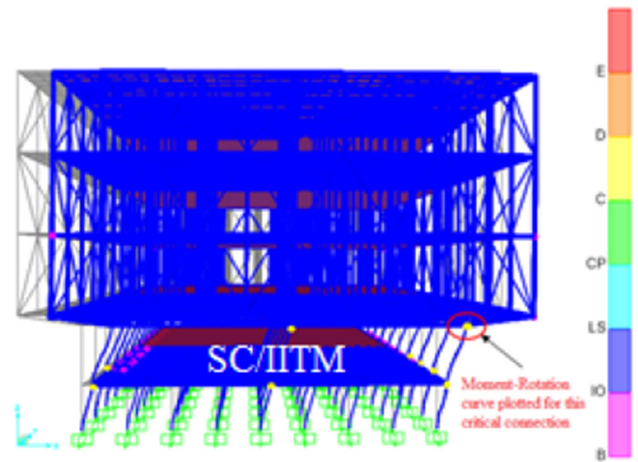


Fig. 35 Collapse pattern of the topside Case-2

based on the topside's maximum roof displacement under combined wave and wind forces [35].

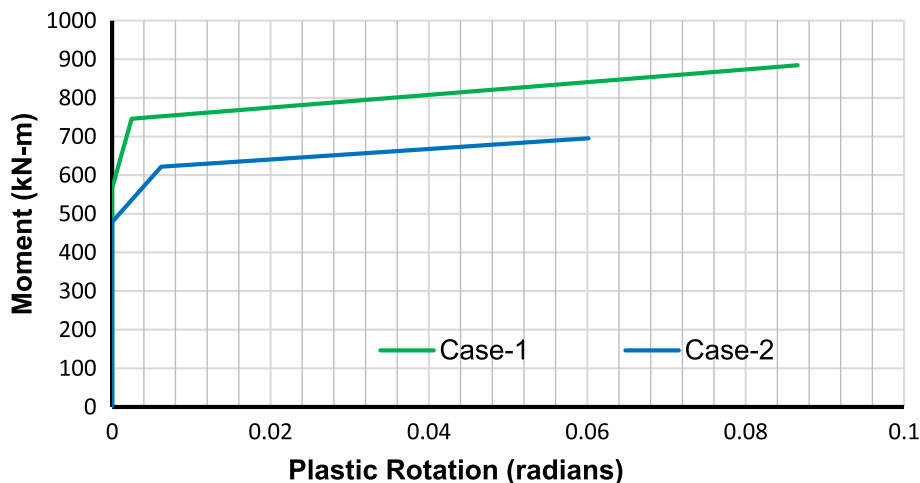
Two cases are considered for the analysis: Case-1, in which FGM is used only on members in regions prone to hydrocarbon explosion while the rest are X-52 steel; Case 2, where X52 steel is used to model the entire topside. Figure 30 shows the pushover curves for different states, namely immediate occupancy (IO), life safety (LS), collapse prevention (CP), and total collapse (C) as per ACT 40 and FEMA 356. A comparison of the capacity curves for cases (1 and 2) is shown in Fig. 31. It is seen that case-1 shows a higher capacity than case-2 (about 8%) because FGM possesses higher yield and ultimate strength in addition to a higher strength ratio, ductility ratio, and tensile toughness; it improved the topside performance under special loads. Bottom-storey columns experienced larger displacement due to the absence of bracings. Variations of stiffness and height resulted in the formation of plastic hinges. Tables 7 and 8

show the different hinge formations on the topside for both cases, while Figs. 32, 33, 34 and 35 show the corresponding hinge locations and topside collapse pattern.

Using FGM in a vulnerable region reduces the number of plastic hinge formations, as shown in Figs. 32 and 33. However, FGM is not recommended for the entire topside considering the complexities involved in the fabrication and economic factors. Figures 34 and 35 show the topside collapse pattern for cases 1 and 2. A comparison of the moment-rotation curve of critical beam-column connection shows that FGM possesses higher resistance to plastic rotation, as shown in Fig. 36, while the moment-rotation values are given in Table 9. It is observed that FGM offers about 21% higher resistance to plastic rotation than X52 steel. The results comparison for cases 1 and 2 are given in Table 10.

In case-1, the maximum number of hinges beyond the yield limit falls within IO (please refer to Table 7), indicating the lesser danger of the topside without losing its original strength. Beam-column connection experiences minor

Fig. 36 Moment-Rotation curve of the connection for Cases-1 and 2



yielding at very few locations (Fig. 32). There is no visible buckling or complete distortion of structural members. It comprises life safety (LS) hinges, topside experiences only moderate damage, retaining some residual strength. Hinges are formed in beam-column connection; however, the shear connection remains sound. Whereas in case 2, the maximum number of hinges falls under life safety (LS). The range of hinges reached Collapse prevention (CP), indicating that the topside experienced severe damage with marginal residual stiffness and strength. The topside suffered permanent deformation, and beams and columns were distorted heavily. Case-2 comprises a few critical joints that come under total collapse (C), affecting the structural integrity, as shown in Fig. 33.

6 Conclusions

The presented study discussed the FGM’s superiority in offshore topside subjected to accidental loads. Topside response under blast load arising from hydrocarbon explosion and impact loads are computed using ABAQUS explicit and designed to withstand the combination of special loads using FGM and X52 steel. The design of the topside under accidental loads satisfied the code recommendations. Nonlinear static pushover analysis is performed to compute the topside capacity using SAP2000. A comparison is made for two cases, namely case-1, where the topside is modelled using FGM only in prone regions, while the rest of the members are with X52 steel. In case 2, where the complete topside is made with X52 steel.

- Numerical analyses showed that the FGM and X52 combination experienced fewer plastic hinges, showing an improved capacity against lateral loading conditions.

Table 9 Moment-rotation values for cases-1 and 2

Steps	Case-1		Case-2	
	Moment (kN-m)	Rotation (radians)	Moment (kN-m)	Rotation (radians)
1	3.3328	0	2.256198	0
2	241.2092	0	157.8793	0
3	486.3068	0	318.1379	0
4	566.3312	0	478.52	0
5	746.042	0.00246	478.52	0
6	750.5084	0.00517	621.883	0.00619
7	768.446	0.016053	632.8165	0.014214
8	804.1636	0.037724	650.1947	0.026967
9	827.1488	0.05167	665.357	0.038094
10	858.0372	0.070411	679.3993	0.048399
11	879.1944	0.083248	691.8169	0.057512

Table 10 Results comparison for cases 1 and 2

Cases	Topside capacity under lateral loading conditions (kN)	Moment resistance at connection (kN-m)	Range of plastic hinge formations
Case-1 (FGM + X52 Steel)	21,822	879	IO, LS
Case-2 (X52 Steel)	20,100	691	IO, LS, CP, C
% Difference	8	21.4	NA

- The range of hinge formations is within immediate occupancy (IO) and life safety (LS), confirming that the topside can retain its original strength.

- On the other hand, the topside made with X52 steel showed severe damage and could not retain residual stiffness and strength.
- Moment-rotation curve at critical beam-column connection showed that the presence of FGM enhances resistance to plastic rotation capacity by about 21% compared to that of X52 steel.
- Using FGM as a structural member in offshore topside proves its suitability for high-pressure and high-temperature applications.

References

- Chandrasekaran, S.; Srivastava, G.: Design aids of offshore structures under special environmental loads including fire resistance. Springer (2018). (ISBN: 978-981-10-7608-4)
- Chandrasekaran, S.: Advanced marine structures. CRC Press (2015). (ISBN: 978-14-987-3968-9)
- Chandrasekaran, S.; Nagavinotini, R.: Offshore Compliant Platforms: Analysis, Design, and Experimental Studies. Wiley (2020). (ISBN: 978-1-119-66977-7)
- Chandrasekaran, S.: Advanced theory on offshore plant FEED engineering, p. 237. Changwon National University, Republic of South Korea (2014). (ISBN: 978-89-969-7928-9)
- Chandrasekaran, S.: Advanced steel design of structures. CRC Press, Florida (2019). (ISBN: 978-036-72-3290-0)
- Chandrasekaran, S.: Parametric studies on the impact response of offshore triceratops in ultra-deep waters. Struct. Infrastruct. Eng. (2020). <https://doi.org/10.1080/15732479.2019.1680707>
- Chandrasekaran, S.; Bhattacharyya, S.K.: Analysis and design of offshore structures with illustrated examples, human resource development center for offshore and plant engineering, p. 285. Changwon National University Press, Changwon (2012). (ISBN: 978-89-963-9155-5)
- Chandrasekaran, S.; Roy, A.: Seismic evaluation of multi-storey RC frame using modal pushover analysis. Nonlinear Dyn. (2006). <https://doi.org/10.1007/s11071-006-8327-6>
- Kaley, P.; Baig, M.A.: Pushover analysis of steel framed building. J. Civ. Eng. Environ. Technol. **4**, 301–306 (2017)
- Kalibhat, M.G.; Kamath, K.; Prasad, S. K.; Pai, R.R.: Seismic performance of concentric braced steel frames from pushover analysis. IOSR J. Mech. Civ. Eng. (IOSR-JMCE), 67–73 (2014)
- Naughton, D.T.; Tsavdaridis, K.D.; Maraveas, C.; Nicolaou, A.: Pushover analysis of steel seismic-resistant frames with reduced web section and reduced beam section connections. Front. Built Environ. (2017). <https://doi.org/10.3389/fbuil.2017.00059>
- Khan, M.I.; Khan, K.N.: Seismic analysis of Steel frame with bracings using pushover analysis. Int. J. Adv. Technol. Eng. Sci. **2**, 369–381 (2014)
- Giordano, A.; Guadagnuolo, M.; Faella, G.: Pushover analysis of plan irregular masonry buildings. In: 14th World Conference on Earthquake Engineering, Beijing, China (2008)
- Elnashai, A.S.: Advanced inelastic static (pushover) analysis for earthquake applications. Struct. Eng. Mech. **12**, 51–70 (2001)
- Chopra, A.K.; Goel, R.K.: A modal pushover analysis procedure for estimating seismic demands for buildings. Earthquake Eng. Struct. Dynam. (2002). <https://doi.org/10.1002/eqe.144>
- Fiore, A.; Spagnoletti, G.; Greco, R.: On the prediction of shear brittle collapse mechanisms due to the infill-frame interaction in RC buildings under pushover analysis. Eng. Struct. (2016). <https://doi.org/10.1016/j.engstruct.2016.04.044>
- Fragiacomo, M.; Dujic, B.; Sustersic, I.: Elastic and ductile design of multi-storey crosslam massive wooden buildings under seismic actions. Eng. Struct. (2011). <https://doi.org/10.1016/j.engstruct.2011.05.020>
- Hasan, R.; Xu, L.; Grierson, D.E.: Push-over analysis for performance-based seismic design. Comput. Struct. (2002). [https://doi.org/10.1016/S0045-7949\(02\)00212-2](https://doi.org/10.1016/S0045-7949(02)00212-2)
- Kaveh, A.; Azar, B.F.; Hadidi, A.; Sorochi, F.R.; Talatahari, S.: Performance-based seismic design of steel frames using ant colony optimization. J. Constr. Steel Res. (2010). <https://doi.org/10.1016/j.jcsr.2009.11.006>
- Clough, L.G.; Clubley, S.K.: Steel column response to thermal and long duration blast loads inside an air blast tunnel. Struct. Infrastruct. Eng. (2019). <https://doi.org/10.1080/15732479.2019.1635627>
- Denny, J.W.; Clubley, S.K.: Evaluating long-duration blast loads on steel columns using computational fluid dynamics. Struct. Infrastruct. Eng. (2019). <https://doi.org/10.1080/15732479.2019.1599966>
- Mahmoudi, M.; Zaree, M.: Evaluating response modification factors of concentrically braced steel frames. J. Constr. Steel Res. (2010). <https://doi.org/10.1016/j.jcsr.2010.04.004>
- Mirjalili, M.R.; Rofooei, F.R.: The modified dynamic-based pushover analysis of steel moment-resisting frames. Struct. Design Tall Spec. Build. (2017). <https://doi.org/10.1002/tal.1378>
- Mwafy, A.M.; Elnashai, A.S.: Static pushover versus dynamic collapse analysis of RC buildings. Eng. Struct. (2001). [https://doi.org/10.1016/S0141-0296\(00\)00068-7](https://doi.org/10.1016/S0141-0296(00)00068-7)
- Pan, X.; Zheng, Z.; Wang, Z.: Estimation of floor response spectra using modified modal pushover analysis. Soil Dyn. Earthq. Eng. (2017). <https://doi.org/10.1016/j.soildyn.2016.10.024>
- Poursha, M.; Khoshnoudian, F.; Moghadam, A.S.: A consecutive modal pushover procedure for nonlinear static analysis of one-way unsymmetric-plan tall building structures. Eng. Struct. (2011). <https://doi.org/10.1016/j.engstruct.2011.04.013>
- Soleimani Amiri, F.; Ghodrati Amiri, G.; Razeghi, H.: Estimation of seismic demands of steel frames subjected to near-fault earthquakes having forward directivity and comparing with pushover analysis results. Struct. Design Tall Spec. Build. (2013). <https://doi.org/10.1002/tal.747>
- Branci, T.; Yahmi, D.; Bouchair, A.; Fourmeley, E.: Evaluation of behavior factor for steel moment-resisting frames. Int. J. Civ. Environ. Eng. (2016). <https://doi.org/10.5281/zenodo.1123588>
- Tarta, G.; Pintea, A.: Seismic evaluation of multi-storey moment-resisting steel frames with stiffness irregularities using standard and advanced pushover methods. Procedia Eng. (2012). <https://doi.org/10.1016/j.proeng.2012.07.123>
- Maddala, P.: Pushover analysis of steel frames. Doctoral dissertation, IIT Madras (2013)
- Simonini, S.; Constantin, R.T.; Rutenberg, A.; Beyer, K.: Pushover analysis of multi-storey cantilever wall systems. In: Proceedings of the 15th World Conference on Earthquake Engineering (2012)
- McInerney, J.B.; Wilson, J.C.: NLTHA and pushover analysis for steel frames with flag-shaped hysteretic braces. In: Proceedings of the 15th World Conference on Earthquake Engineering, Lisbon, Portugal, 24–28 (2012)
- Tang, Z.; Wei, T.; Ma, Y.; Chen, L.: Residual strength of steel structures after fire events considering material damages. Arab. J. Sci. Eng. (2019). <https://doi.org/10.1007/s13369-018-03711-8>
- Raheem, S.E.A.: Study on nonlinear response of steel fixed offshore platform under environmental loads. Arab. J. Sci. Eng. (2014). <https://doi.org/10.1007/s13369-014-1148-x>
- Chandrasekaran, S.; Pachaiappan, S.: Numerical analysis and preliminary design of topside of an offshore platform using FGM and

- X52 steel under special loads. *Innov. Infrastruct. Solut.* (2020). <https://doi.org/10.1007/s41062-020-00337-4>
36. Chandrasekaran, S.: Design of Marine Risers with Functionally Graded Materials, p. 200. Woodhead Publishing, Elsevier (2020). (ISBN: 978-0128235379)
37. Chandrasekaran, S.; Hari, S.; Amirthalingam, M.: Wire arc additive manufacturing of functionally graded material for marine risers. *Mater. Sci. Eng. A* (2020). <https://doi.org/10.1016/j.msea.2020.139530>
38. IS:875- Part 1 and II (1987). Code of Practice for design loads, Bureau of Indian Standards, New Delhi, India.
39. Kumar, K.; Surendran, S.: Design and analysis of composite panel for impact loads in marine environment. *Ships Offshore Struct.* (2013). <https://doi.org/10.1080/17445302.2012.736362>
40. Liew, J.R.; Sohel, K.M.A.; Koh, C.G.: Impact tests on steel–concrete–steel sandwich beams with a lightweight concrete core. *Eng. Struct.* (2009). <https://doi.org/10.1016/j.engstruct.2009.03.007>
41. Shivakumar, K.N., Elber, W., & Illg, W.: Prediction of impact force and duration due to low-velocity impact on circular composite laminates (1985). <https://doi.org/10.1115/1.3169120>
42. Zucchelli, A.; Minak, G.; Ghelli, D.: Low-velocity impact behaviour of vitreous-enameled steel plates. *Int. J. Impact Eng.* (2010). <https://doi.org/10.1016/j.ijimpeng.2009.12.003>
43. Pachaiappan, S.; Chandrasekaran, S.: Numerical analysis of offshore topside with FGM under impact loads. *Innov. Infrastruct. Solut.* (2022). <https://doi.org/10.1007/s41062-022-00802-2>

Springer Nature or its licensor (e.g. a society or other partner) holds exclusive rights to this article under a publishing agreement with the author(s) or other rightsholder(s); author self-archiving of the accepted manuscript version of this article is solely governed by the terms of such publishing agreement and applicable law.

